Swash-by-swash morphology change on a dynamic cobble berm revetment: high-resolution cross-shore measurements

Paul Bayle, Chris E. Blenkinsopp, Kévin Martins, George Kaminsky, Heather Weiner, David Cottrell

Swash-by-swash morphology change on a dynamic cobble berm revetment: high-resolution cross-shore measurements.

Paul M. Bayle, (p.m.bayle@bath.ac.uk)[a,e], Chris E. Blenkinsopp, (cb761@bath.ac.uk)[a], Kévin Martins, (kevin.martins@u-bordeaux.fr)[c], George M. Kaminsky, (george.kaminsky@ecy.wa.gov)[b], Heather M. Weiner, (heather.weiner@ecy.wa.gov)[b], David Cottrell, (cranberrydavid@yahoo.com)[d]

[a] *Centre for Infrastructure, Geotechnics and Water Engineering, Department of Architecture and Civil Engineering, University of Bath, Bath, BA2 7AY, UK*
[b] *Washington State Department of Ecology, Olympia, Washington, USA*
[c] *UMR 5805 EPOC, CNRS - University of Bordeaux, F-33600 Pessac, France*
[d] *Pacific County Drainage District 1, North Cove, Washington, United States of America*
[e] *Currently: Delft University of Technology, Faculty of Civil Engineering and GeoSciences, Department of Hydraulic Engineering, Stevinweg 1, 2628CN, Delft, The Netherlands*

Abstract

Dynamic cobble berm revetments are a promising soft engineering technique capable of protecting sandy coastlines by armouring the sand and dissipating wave energy to protect the hinterland against wave attack. They also form composite beaches as they are essentially mimicking natural composite beach structure and behaviour. This type of coastal protections and beaches have recently been investigated, and this led to a better understanding of their overall behaviour under varying water levels and wave conditions. However, the short-term dynamics of the wash zone (where all bed changes occur) has never been studied at high-resolution, and this is needed to fully understand the underlying dynamics of such structures and relate it to observed processes at larger scale. To do so, the revetment at North Cove (WA, USA) was monitored for a nine-day period in January 2019 over a spring tidal cycle and with significant wave heights offshore reaching 6 m. A 2-D lidar was used to survey a cross-shore profile of the revetment, and record all surface changes and interaction with swashes at high spatial (0.1 m) and temporal (swash-by-swash) resolution. The revetment was found to rapidly reshape under these energetic conditions, but reached a relatively stable state during the rising tide. The analysis of bed-level changes and net cross-shore mass fluxes over the revetment showed that revetment changes are mainly driven by very small events, with some rare large bed-level changes of a magnitude comparable to the median cobble diameter. The distribution of event mass fluxes nearly balanced out over the duration of a tide, meaning that positive and negative fluxes tended to be symmetrical. Furthermore, measured net fluxes magnitude were 18 times smaller than the absolute fluxes, which demonstrated the dynamic stability of the revetment as substantial movement occur on a wave-by-wave timescale but these balance out over time. The analysis of swash revealed that the revetment section where the swash reaches a maximum depth between $0.15 - 0.45$ m undergoes the more extreme fluxes. Swashes deeper than 0.45 m only occurred in zones inundated more than 50 % of the time, and smaller extreme fluxes were measured over the revetment section where these deep swashes were recorded. Bed level change oscillations over the revetment were observed, and the cross shore limit of these was correlated with the mean wave period at the toe of the revetment. Overall, the water depth at the toe of the revetment was identified as the key parameter to describe the energy reaching the revetment. This study enables the morphodynamics

of dynamic revetment, observed in previous lab and field studies, to be explained at the swash scale, and brought new information on the sediment dynamics of composite beaches and dynamic revetments. These findings allow to suggest some generic guidance for dynamic cobble berm revetment design. Finally, the results are compared to a similar study on sandy beaches.

Keywords:

Dynamic Cobble Berm Revetment; Lidar; Swash processes; Sediment fluxes; Morphodynamics

1. Introduction

Dynamic cobble berm revetments are a type of soft engineering technique intended to protect sandy coastlines against erosion and flooding (Allan et al., 2006; Allan & Gabel, 2016; Bayle et al., 2020). Dynamic cobble berm revetments are a sub-category of dynamic revetments which specifically aim to create an artificial composite beach, which consists of a lower sandy foreshore and a backshore berm or ridge composed of gravels. The gravel ridge is a highly-dynamic feature that armours the underlying sand (Bayle et al., 2020, 2021) and provides overtopping protection to the hinterland (Allan et al., 2006; Komar & Allan, 2010; Loman et al., 2010; Allan et al., 2012, 2005; Allan & Gabel, 2016; Blenkinsopp et al., 2022a). Composite beaches have long been recognised as an effective form of natural coastal protection (*e.g.*, see Ahrens, 1990; Allan & Gabel, 2016), showing a great degree of stability and adaptability in response to wave attack (Van Rijn, 2010). Although these coastal landforms are ubiquitous in some regions of the globe (Kirk, 1980), they have received much less attention than purely sand or gravel beaches. In addition, while the concept of dynamic revetments is not new (*e.g.*, van der Meer & Pilarczyk, 1986; Powell, 1988; Lorang, 1991; Ward & Ahrens, 1992; Komar & Allan, 2010, and many others), examples of application in the field are scarce and monitoring programs of existing structures are very limited (Bayle et al., 2020). As a consequence, there is an overall lack of understanding of dynamic cobble berm revetments and composite beaches dynamics, and their behaviour under the combined effect of varying water levels and wave conditions is not well documented.

Dynamic cobble berm revetments (and gravel ridges of composite beaches) are in some aspects similar to that of pure gravel beaches. They are both predominantly influenced by swash processes which can generate significant changes in both the cross-shore and longshore direction over short time scales (Jennings & Schulmeister, 2002). They are also both highly porous, resulting in substantial infiltration/exfiltration of water through the gravel under swash motion (Holland, 2019). While many studies have contributed to a better understanding of wave-by-wave swash dynamics and gravel transport on pure gravel beaches (*e.g.*, Carter & Orford, 1984; Williams et al., 2009; Poate et al., 2015; Almeida et al., 2015), equivalent studies on composite beaches or dynamic cobble berm revetments are rare. Yet, such short-term analyses of the swash zone are important for dynamic revetment and composite beach research because the gravel component of the beach differs from a pure gravel beach as it is founded on a relatively impermeable sand layer (Jennings & Shulmeister, 2002). Consequently, study of the morphodynamics of dynamic cobble berm revetments at the swash-by-swash time scale is useful to better understand the global behaviour of these structures. In parallel, while longshore sediment transport plays an important role in the long-term erosion trend at the site, cross-shore sediment transport dominates at the short-term swash-by-swash time scale during high energy wave events as is typically the case for pure sand (*e.g.*, Blenkinsopp et al., 2010, 2011) and gravel beaches (*e.g.*, Williams et al., 2009; Almeida et al., 2015). Therefore, similar cross-shore high-resolution investigation of composite beach/dynamic cobble berm revetment morphodynamics is beneficial for scientists and engineers.

Dynamic cobble berm revetments and composite beach ridges are by essence composed of three layers: 1) A layer of pure gravels, which generally behaves like a pure gravel beach. This layer is subjected to long- and cross-shore transport, which over time, tends to generate a net landward transport of particles(Carter

& Orford, 1984). Cross-shore sorting of particles in the pure gravel layer is common, with the direction of sorting dependent on the hydrodynamic capacity of the swash to bring the largest particles into motion (Bluck, 1967; Orford, 1975; Williams & Caldwell, 1988; Bayle et al., 2021). 2) A layer of mixed gravel and sand, composed of coarse sand and small pebbles. This layer is vertically sorted, with particle size decreasing with depth (Pye & Blott, 2018). 3) A layer of pure sand. The presence of these three layers makes the hydraulic conductivity and water table of a beach with a dynamic revetment or a composite beach different from pure gravel beaches, and is expected to influence the swash dynamics (Holland, 2019; Blenkinsopp et al., 2022b). The swash motions at the wave-by-wave scale cause rearrangement of surface particles, which can in turn lead to temporary exposure and movement of underlying gravel and sand. In addition, sand beneath the cobbles can be eroded by the water percolating through the permeable pure gravel layer (Bayle et al., 2021); it can also accumulate and compact due to kinetic sieving, which results from the vibratory mechanism of the swash (Wright et al., 1982). In tidal environments, the tide level plays a key role in the dynamics of composite beaches as hydrodynamic conditions change from dissipative at low and mid tide (shoreline on the mildly sloping sand beach face) to reflective conditions around high tide, when the swashes interact with the much steeper gravel berm (Blenkinsopp et al., 2022b). These processes were investigated through both a laboratory (Bayle et al., 2020) and field study (Bayle et al., 2021) and provided physical explanations of the overall dynamics and stability of dynamic revetment and composite beaches. Here we investigate cross-shore processes at the swash-by-swash scale to better understand swash zone morphodynamics of dynamic cobble berm revetments and composite beach ridges, and when possible, relate them to observed processes at larger scale.

To address the aforementioned points and better understand the dynamics of dynamic revetments and composite beaches, the present study investigates for the first time swash processes and swash-induced sediment mass fluxes on a dynamic cobble berm revetment. The analysis is performed at temporal scales ranging from seconds to the tidal timescale, so that observed changes are put in perspective with hydrodynamic forcing. The study uses high-resolution hydrodynamic and topographic measurements collected using a 2-D lidar scanner along a cross-shore transect of the dynamic cobble berm revetment in North Cove, Washington State, USA (Kaminsky et al., 2020). The field experiment was performed over a nine-day period around a spring tide in January 2019, during energetic wave conditions at a location with a history of extreme erosion (Kaminsky et al., 2010).

The paper is structured as follows: Section 2 presents the methodology, including a description of the study area, the lidar setup, the environmental conditions during the experiment and the data processing techniques. Section 3 presents the swash analysis of cross-shore mass fluxes. Section 4 discusses the results in terms of sediment transport, and compares the main findings with a similar study on sandy beaches. Finally, Section 5 concludes and suggests potential future work.

2. Methodology

2.1. Study Site

The town of North Cove is situated on the U.S. Pacific northwest coast along the northern shore of the Willapa Bay entrance in Washington State (see Figure 1a). This open sandy coast faces the Pacific

ocean and is therefore exposed to a severe wave climate, particularly in winter with storms producing deep-water significant wave heights greater than 10 m at least once a year (Allan & Komar, 2002; Ruggiero et al., 2005; Michalsen, 2018). Semi-diurnal tides dominate this part of the coastline, with a tidal range ranging from 2 to 4 m (Kaminsky et al., 2010). Ocean waves entering the bay drive longshore sediment transport toward the southeast, which may be enhanced by the flood tide. Wind waves from the south generated within the bay can drive nearshore sediment transport toward the northwest, aided by the ebb tide (Lesser, 2009). The combination of energetic hydrodynamics, storm events and northward migration of the main tidal channel within the inlet has led to chronic coastal erosion at North Cove over several decades, with an average recession estimated at 20 m/yr between 1950 and 1999 (Kaminsky et al., 2010). A maximum rate of recession of 37.3 m/yr was observed between 1963 and 1974. 37.3 m/yr was observed between 1963 and 1974. At the beginning of the 21^{st} century, this reduced to approximately 13 m/yr. More details on the overall sediment transport processes along the coast can be found in Kaminsky et al. (2010) and Bayle et al. (2021).

Following existing examples of dynamic revetments constructed along the west coast of the USA (Allan & Gabel, 2016; Allan et al., 2012, 2005), the extreme erosion at North Cove motivated the installation of a dynamic cobble berm revetment to protect the coastline from further erosion. The complete history of the site, the description of the initial placement and the detailed beach and revetment state can be found in Bayle et al. (2021), section 2.1. Starting in February 2017, an ad-hoc revetment was built using angular and poorly sorted rock from a local quarry. The material has a diameter range varying from a few centimetres to almost one metre ($D_{50} = 0.15$ m) and is primarily basalt with a bulk density of 1830 kg/m^3, although other type of rock can be found. The hardness of the material means that it tends to fracture and abrade into smaller pieces, reducing the D_{50} over time, and adding coarse sand to the material range. The revetment material is therefore very heterogeneous in terms of shape and size, and the angularity of the material facilitates interlocking in comparison with more rounded shingle often found on composite beaches. For the remainder of this paper, the construction material will be referenced as 'cobbles', as this characterises the predominant material size within the revetment. Cobbles were placed incrementally over time to reach a total volume of 16.23 m^3/m around the monitoring site (Figure 1a). At the experiment location, the revetment has a cross-shore width of approximately 20 m in winter (storm season). The revetment reached its present condition (gross shape, width and elevation) rapidly after instalment (in the order of days), however it remains dynamic in essence as its shape and slope continuously change (Bayle et al., 2021). Wave action over time has led to cross-shore sorting, with cobble size decreasing landward. Due to the presence of this revetment, the beach is considered to be an artificial composite beach: cobbles composing the upper ridge are in direct interaction with waves at mid and high tide (Figure 1c); at low tide, the shoreline is typically around 120 m seaward of the cobble toe, and the sub-aerial beach is dominated by sand (Figure 1b) with a D_{50} of about 0.18 mm (Kaminsky et al., 2010).

The revetment at North Cove was chosen as the study site for this experiment because examples of dynamic cobble berm revetments are rare and there is a thorough ongoing monitoring programme being undertaken at the site (Weiner et al., 2019; Kaminsky et al., 2020) which this experiment was timed to

Figure 1: (a) Geographical location of the North Cove dynamic cobble berm revetment. The Grays Harbor Waverider buoy is shown as a yellow triangle, and the Toke Point tide station as a green circle, in the bottom left map. (b) Photographs of the dynamic revetment on the 24/01/2019 at low tide; (c) Photographs of the dynamic revetment on the 21/01/2019 at mid-tide (during flood). Note that the top of the revetment is delimited by an artificial drift log barrier. Under very high water levels and energetic conditions, the maximum runup limit reaches this log barrier. *Photos taken by Paul Bayle.*

coincide with.

2.2. Field experiment

The field experiment was performed over nine days, from 17/01/2019 to 25/01/2019, around the second spring tide of January. This monitoring period will be referred to as "spring tidal cycle" for the remainder of the paper. The principal motivation of the experiment was to collect comprehensive data which captured the morphological evolution of the dynamic revetment over the study area shown in Figure 1a in order to analyse the behaviour and dynamics of the revetment. The overall revetment topographic evolution was surveyed with Real-Time Kinematic Global Navigation Satellite System (RTK-GNSS) and individual cobbles were tracked with Radio Frequency Identification (RFID, *e.g.* see Weiner et al., 2019). The analysis performed by (Bayle et al., 2021) revealed that the revetment remained a coherent structure over the spring tidal cycle, only losing an average of $0.67\,\mathrm{m}^3/\mathrm{m}$ over the study area.

This volume loss was mainly associated with sand erosion from within or beneath the cobbles since no cobbles were transported seaward of the revetment toe. Figure 4e shows an example of the pure cobble and mixed sand and cobble layer resting on pure sand. All profiles and available pure cobble layer thickness recorded during the experiment are presented in Figure 8 and 9 in Bayle et al. (2021), along with a conceptual model of layer thickness evolution. The present contribution focuses on swash-driven cross-shore fluxes studied at the scale of individual swash events using high-resolution hydrodynamic and topographic data from a 2-D lidar which captured high-frequency revetment profile data along a single cross-shore transect (Figure 1a).

(a)

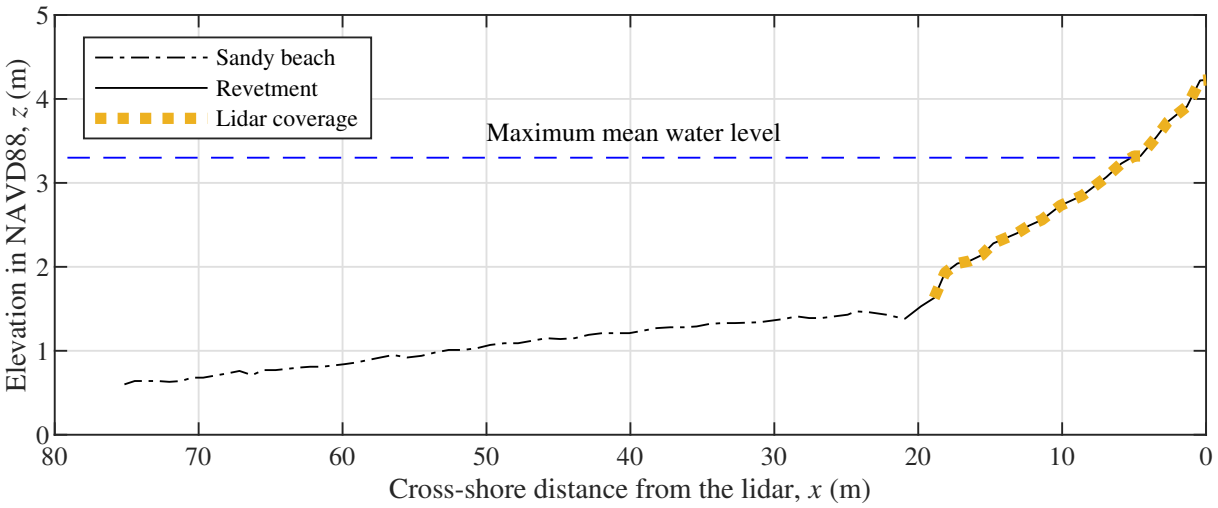

(b)

Figure 2: (a) Photographs of the lidar deployment. The left-hand image was taken at low tide along the lidar transect looking landward. The right-hand image shows the lidar when recording during a high tide, looking alongshore. The central photograph shows a close-up of the lidar mounting system. (b) Cross-shore profile of the beach along the lidar transect measured using RTK-GNSS. Note that the minimum water level recorded by the tide gauge (Figure 1a) during the experiment was $z = -1$ m referenced to the North American Vertical Datum 1988 (NAVD88), and therefore is not represented on the figure. *Photos taken by George Kaminsky, Heather Weiner, and Paul Bayle*

A SICK LMS 511 lidar scanner was deployed for this experiment, and was mounted on top of a 6 m-pole strongly attached to a large drift log at the top of the revetment. The pole and lidar were anchored with four guy lines making it nearly immobile even in strong winds (Figure 2a). The lidar collected

free surface elevation and revetment profile measurements along a 18.7 m-long 2D cross-shore transect of the cobble revetment (Figure 2b) for approximately six hours around each high tide of the spring cycle (three hours before and after) to capture interactions between waves and cobbles. The lidar collected data at 25 Hz with an angular resolution of 0.1667° across a 150° field-of-view. In the remainder of the paper, the cross-shore data are given relative to the lidar position, with the distance x increasing seaward. Elevations z are given relative to the North American Vertical Datum 1988 (NAVD88).

The height of the lidar was chosen so that its swath covered most of the revetment section while keeping a high spatial resolution. In this configuration, the lidar is high enough for its signal not to be affected by shadowing of cobbles (only very large cobbles at the toe could sometimes create a shadow area, but this area was smaller than the grid size used – 0.1 m see Section 2.4.1). The horizontal resolution of the lidar decreases with distance (Almeida et al., 2015), therefore the horizontal resolution at the toe of the revetment must be kept below or equal to the grid size. The configuration and height reported here provided a horizontal resolution ranging from 2 cm right below the lidar to 10 cm at the seaward edge of the revetment profile. The vertical resolution of the lidar is 1 mm, and this in constant in space over the range used in this study.

2.3. Environmental Conditions

The weather conditions during the experiment were obtained from publicly available continuously operating stations. Water levels were obtained for the Toke Point station (station 9440910; Figure 1a) from the NOAA tides and currents open data platform. The validated version of the data is used in this study. Wave height, period, and direction were obtained from the Coastal Data Information Program (CDIP) Grays Harbor Waverider buoy (station 46211; Figure 1a) from the NOAA National Data Buoy Center open-source platform. Figure 3 shows the timeseries of wave and water-level data for the duration of the field experiment: wave data were available every half hour (Figure 3a and b); and water level data every six minutes (Figure 3c). The wave conditions during the spring tidal cycle were characterised by large and long-period swell wave conditions, peaking at $H_s = 6$ m and $T_p = 15$ s on 19/1 at the Waverider buoy. During the experiment, although incident waves came from varying directions (west and south-west) at the Waverider buoy, the configuration of the studied site (orientation and very dissipative beach) mean the dynamic revetment is swash-aligned, generating approximately alongshore uniform longshore transport (Kaminsky et al., 2020; Bayle et al., 2021).

2.4. Lidar data processing

2.4.1. Separation of hydrodynamic and topographic measurements

The lidar dataset was first converted from polar to cartesian coordinates, despiked and interpolated onto a 0.1 m horizontal grid (*e.g.*, see Almeida et al., 2015; Martins et al., 2016, 2017). The output from this process is a series of timeseries of yet non separated bed and swash surface elevations at 0.1 m cross-shore intervals. At each location, the "bed" elevation (when the swash depth is zero) and "swash" elevation data were separated following Almeida et al. (2015) and Martins et al. (2016). This methodology, based on the technique proposed by Turner et al. (2008) for ultrasonic bed-level sensors, starts by computing the variance of the elevation timeseries over a moving 4 s window at each cross-shore

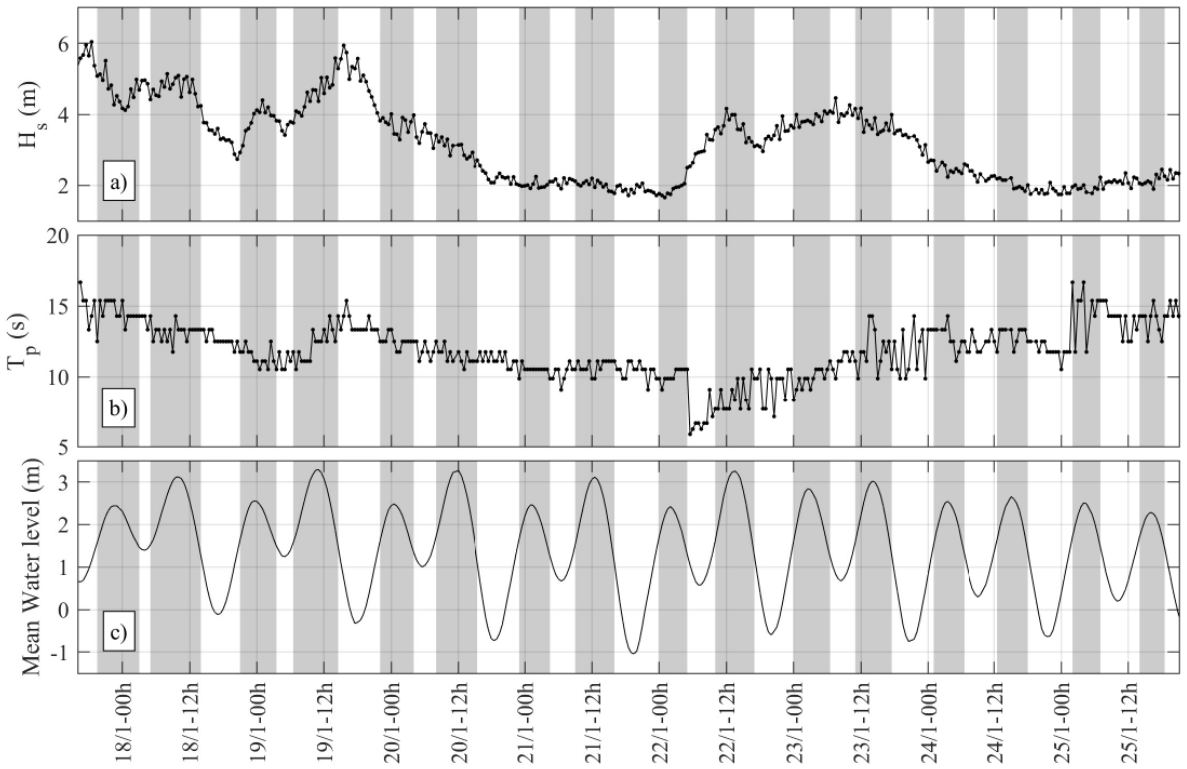

Figure 3: Timeseries of: (a) Significant wave height, H_s (m); (b) Peak wave period T_p (s); and (c) Mean water level (m) relative to the NAVD88 datum. The shaded areas indicate when the Lidar was recording during mid- and high tides, which corresponds to periods when there was swash interaction with the revetment (from collision regime to overwash regime, Sallenger (2000)). Times are given in Pacific Time (GMT-8).

location (*i.e.*, at each grid point). The median of the variance over the tide is then calculated for each grid point, and used as a threshold below which points are considered as stationary (corresponding to the bed). The threshold therefore varies with cross-shore distance from the lidar, as suggested by Almeida et al. (2015), which minimises the error associated with horizontal resolution. A minimum value of 0.0002 m^2 for at least 2.4 s was set as the threshold for bed detection. Figure 4 shows an example of this separation process over a four–minute window at four cross-shore locations across the revetment. Note that the bed elevation measured with the lidar only corresponds to the cobble surface and does not capture the sandy beach seaward of the revetment toe. Figure 4e shows the profile measured after the 22/1-10h high tide, including measured of layers thickness. 'Note that the revetment is a low volume revetment which effectively consists of a few layers of pure cobbles, but it was shown to have a valid coastal protection function (Bayle et al., 2021). Further post-processing of the separated bed/swash elevation data enables the instantaneous shoreline position, which is defined at the most landward point where the swash depth is larger than 0 m, to be tracked in both time and space enabling extraction of the runup and rundown limits (Blenkinsopp et al., 2022b).

2.4.2. Definition of individual swash events

The same nomenclature as in Blenkinsopp et al. (2011) is used hereafter to refer to swash terminology. Following Hughes & Moseley (2007), individual swash events correspond to an inundation event between consecutive occurrences of a dry bed at a fixed location in space. As illustrated in Figure 4, each swash

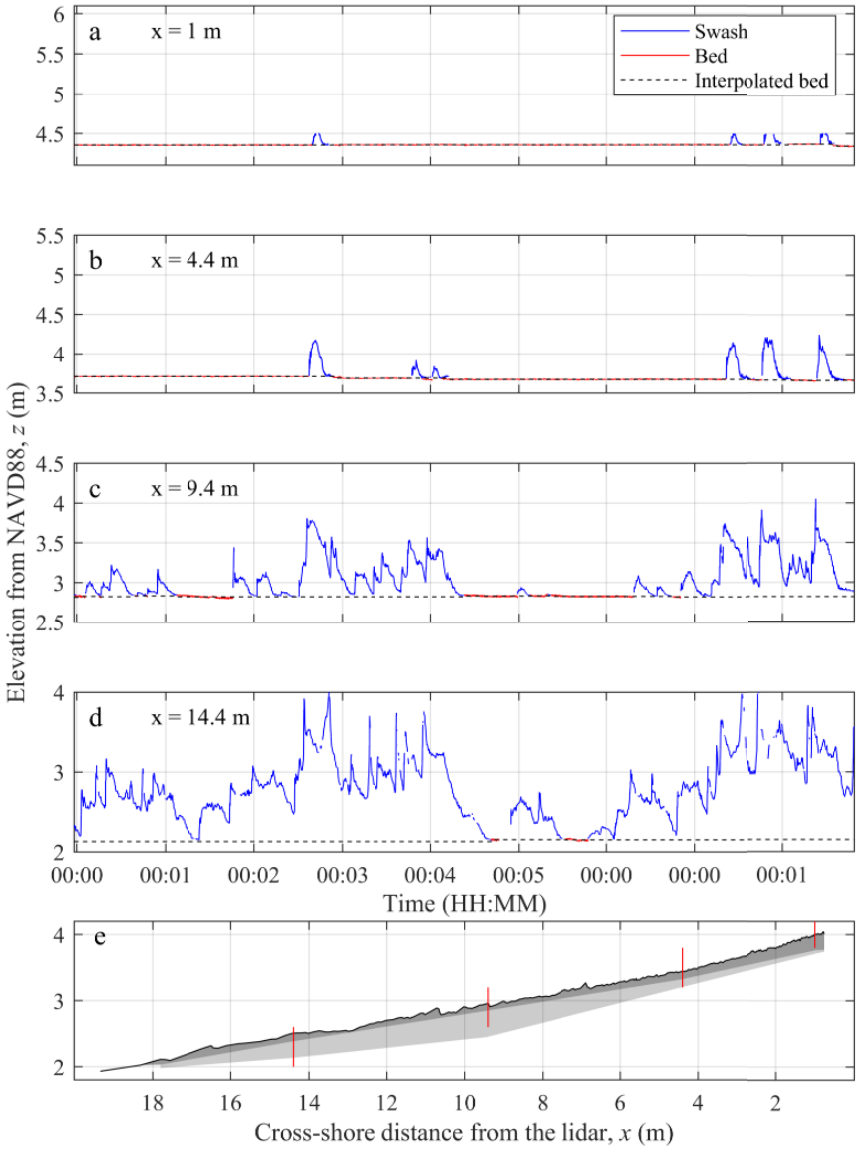

Figure 4: Example of "swash" and "bed" extraction over a four-minute window, extracted at 07:48 during the 18/01/2019 high tide, at (a) $x = 1\,\mathrm{m}$, (b) $x = 4.4\,\mathrm{m}$, (c) $x = 9.4\,\mathrm{m}$ and (d) $x = 14.4\,\mathrm{m}$. Blue lines represent the "swash" timeseries, red lines the "bed" timeseries and dashed black lines the continuous and "interpolated bed" timeseries. The position of each cross-shore point presented in (a-d) are shown by red bar on (e), where a cross-section of the revetment after 22/1-10h tide is shown. The dark and light shaded area represent respectively the pure cobble layer and the mixed sand and cobble layer found above pure sand.

event can be composed of several incident waves/bores, defined by local maxima in the swash elevation timeseries. Since at high tide, the most seaward locations in the lidar transect can be continuously submerged, a maximum of 25 bores were allowed per individual swash event. This method and threshold was successfully used in Blenkinsopp et al. (2011) to identify swashes with long duration which are considered more characteristic of the inner surf zone, and this approach was found to perform well for the current analysis.

2.4.3. Net cross-shore mass flux

Using the "bed" timeseries, the net bed-level changes caused by each swash event were computed for each cross-shore lidar measurement position using the bed elevation immediately before and after that

event. The net cross-shore mass flux per swash event past any point on the revetment face is directly obtained from these bed-level changes at each discrete point on the revetment surface, and will be referred to as "event mass flux" and noted Q_{event} for the remainder of the paper. The volume flux per metre of coastline $q(x')$ (positive onshore) past the cross-shore location x' for each swash event is given by:

$$q(x') = \int_{x'}^{x_0} \Delta z(x) dx \tag{1}$$

given in m^3/m, where x_0 is the lidar position (*i.e.*, $q(x_0) = 0$, as the drift log barrier prevents any transport further this point), Δz is the bed-level change at each lidar grid point (m) and dx is the cross-shore spacing between each grid point (0.1 m). The corresponding event mass flux per metre of coastline, $Q(x')$ (positive onshore) is then given by:

$$Q_{event}(x') = \rho_b q(x') \tag{2}$$

given in kg/m, where ρ_b is the bulk mass density ($\rho_b = 1830$ kg/m^3). This method has previously been applied by Blenkinsopp et al. (2011) in a field experiment investigating swash processes on a sandy beach. It was also illustrated for multiple events in Turner et al. (2009).

The experimental data allow the event mass flux, which includes both sand and cobble transport (suspended sand within swashes could not be separated from cobbles) to be quantified for all individual swash events acting on the revetment. Furthermore, knowing the duration of each swash, the net cross-shore mass flux per second was calculated by simply dividing the event mass flux by the duration of the swash. The obtained mass flux rate per metre of coastline, given in kg/(sm), will be referred to as the "mass flux" (as opposed to the previous "event mass flux") for the remainder of the paper, and noted as Q_s.

3. Results

All the recorded tide used for the analysis are shown in Table 1. The results section is separated into two subsections: the first subsection will present an "example tide" (19/1-17h, Table 1) to (1) illustrate the analysis that was done for all tides, and (2) demonstrate consistent behaviour observed during all tides important for understanding the observed swash-induced bed level changes; the second subsection will focus on the bulk analysis of the swash and fluxes of all tides combined. Note that two tides (18/1-19h and 19/1-08h) are not used for the bulk analysis because several large cobbles were manually placed and removed along the lidar measurement transect, which would lead to a bias in the analysis.

3.1. Observed cross-shore revetment dynamics

For the following analysis, the data from the overnight high tide on 19/1 are used. During this tide, the offshore wave height, wave period and mean water level reached a maximum of 4.05 m, 13.3 s and 2.48 m respectively, which rank this tide fifth out of the 16 high tides recorded in terms of offshore wave power (therefore this tide is also representative of the energetic conditions over the spring tidal cycle). This tide will be referred to as "the example tide" for the remainder of the paper.

Table 1: Mean offshore wave energy (E), mean wave energy (E_{toe}) and mean wave period ($T_{m02,toe}$) at the toe of the revetment during the 14 tides used in this paper. The data at the toe of the revetment were calculated at high tide when the lidar measurements at the toe of the revetment corresponded to the surf zone. Those data could not be obtained accurately for the 17/1–18h. Q_{net} is the net cross-shore mass flux measured over the entire tide at the maximum mean shoreline position for each high tide. Q_{abs} is the sum of the absolute value of all fluxes measured at the same position as Q_{net}. The last two variables are used in Section 4.2.

Tide	E	E_{toe}	$T_{m02,toe}$	Q_{net}	Q_{abs}
(DD/M-hh)	(kJ/m^2)	(kJ/m^2)	**(s)**	(kg/m)	$kg/m)$
17/1–18h	27.88	-	-	-	-
18/1–07h	28.81	1.65	4.48	-1692	5040
19/1–21h	17.47	1.12	4.21	251	2161
20/1–08h	11.81	1.39	3.66	-359	602
20/1–23h	5.11	0.82	3.37	136	916
21/1–08h	5.23	1.40	4.72	110	991
21/1–23h	4.39	0.59	2.94	-39	97
22/1–10h	16.94	1.27	3.72	67	2328
23/1–01h	18.83	0.93	3.76	-74	2171
23/1–10h	17.76	1.22	3.56	-202	922
23/1–23h	7.70	0.83	3.59	174	1284
24/1–12h	5.35	0.85	3.20	110	921
24/1–23h	4.66	0.75	3.25	-118	979
25/1–12h	5.82	0.86	3.64	6	1301

3.1.1. Bed-level changes and net cross-shore mass flux

Using the "bed" timeseries (Section 2.4.1), net bed-level changes relative to the revetment face morphology at the start of the timeseries were computed every second at each cross-shore position on the 0.1 m grid. Figure 5 shows the morphological evolution of the revetment face through the example tide over the whole revetment width, where red marks erosion and blue accretion. Note that Figure 5 is used to contextualise the analysis performed, but nonetheless, the pattern of accretion in the upper swash and erosion in the lower swash is recurrent in all recorded tides (see Figure 8 and 9 in Bayle et al., 2021).

Figure 6a presents percentage occurrence distributions of bed-level changes per individual swash event at three locations across the revetment face. The majority of swashes induced a net bed-level change smaller than ±3 cm at all three locations. The same analysis was completed for all tides with similar results. The distribution in the upper part of the revetment at $x = 6.4$ m is wider, indicating larger bed-level changes in the upper part of the revetment due to the presence of small cobbles (grading decreasing landward). The maximum swash-induced net bed-level change was +6 cm during the example tide, and −14 cm over all tides. Note that these changes are well outside the range displayed in Figure 6a. Notably, these large single-event bed-level changes are of the same order of magnitude as the total net morphological change at any point on the revetment. Figure 6b shows the percentage occurrence of event mass fluxes,

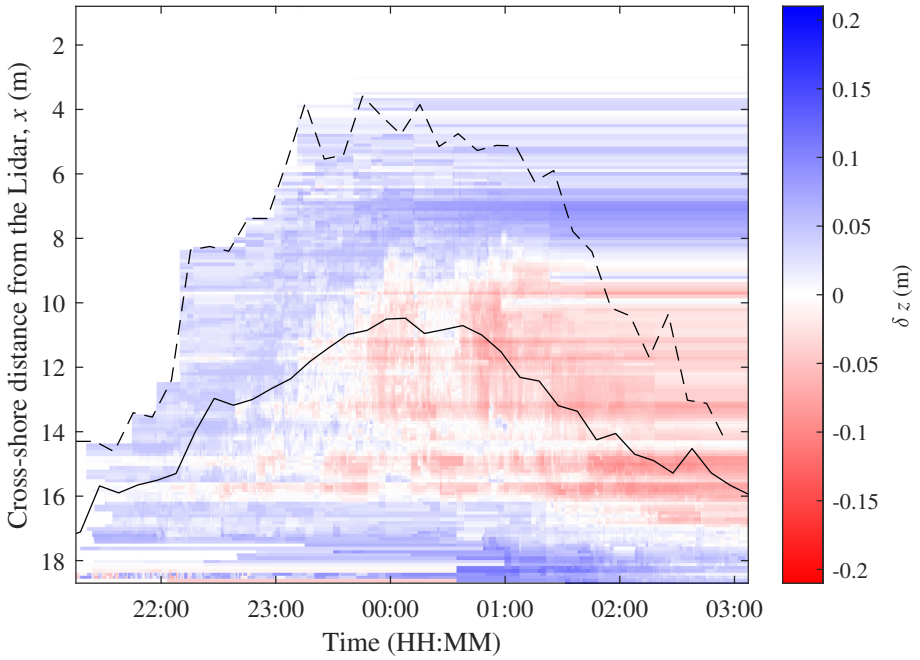

Figure 5: Change in bed-level through the swash zone during the example tide, measured using the lidar (the magnitude of x increases in the offshore direction). The dashed and solid lines represent the runup limit and the mean shoreline position respectively. The colour scheme represents net bed-level change in metres relative to the revetment face morphology at the start of the timeseries. The net morphological change swash zone over the example tide is characterised by accretion of up to 21 cm. Note that the drift log barrier (Figure 1c and Figure 2a) is at $x = 0.7$ m.

recorded at the same three cross-shore locations as in Figure 6a. Similar distribution is obtained, and the standard deviation is smaller on the upper beach face, with the average value over all tides varying from 9.7 kg/m per swash at $x = 6.4$ m to 17.1 kg/m per swash at $x = 14.4$ m. Rare events produced large event mass fluxes, with a maximum of +180 kg/m during the example tide, and −233 kg/m over all recorded tides. The results shown in Figure 6b are almost symmetrically distributed, and a similar distribution is observed for all tides, whether they experienced net erosion or accretion. This suggests that the volume changes caused by cobble transport over hundreds of swash events almost balance over longer time scales. The resulting net bed level change or flux at a specific location can be due to either the sum of slight imbalance between positive and negative swashes or few extremes events. This will be discussed further in Section 3.2.1 and in the discussion section of this paper.

The zero-equivalent swash-induced bed-level changes represented by the central bar on Figure 6 also tends to vary across-shore. However, due to the vertical precision of the lidar (±1 mm, Section 2.2), a quantitative interpretation cannot be performed with high confidence within this range and is the reason why only the analysis of the distribution over the whole range plotted in Figure 6 was discussed above.

3.1.2. Rates of bed volume change

The balance of onshore and offshore sediment fluxes observed in Figure 6 is further illustrated in Figure 7. In this figure, the "net" and "gross" rate of bed volume change as defined in Bayle et al. (2020) is used. The "net" volume change (per metre width) per second represents the rate of volume change over ten minutes, denoted dV_{10}, which is effectively the mean rate of change over ten minutes. The "gross" volume change (per metre width) per second, denoted $\overline{dV}$, is quantified by summing the

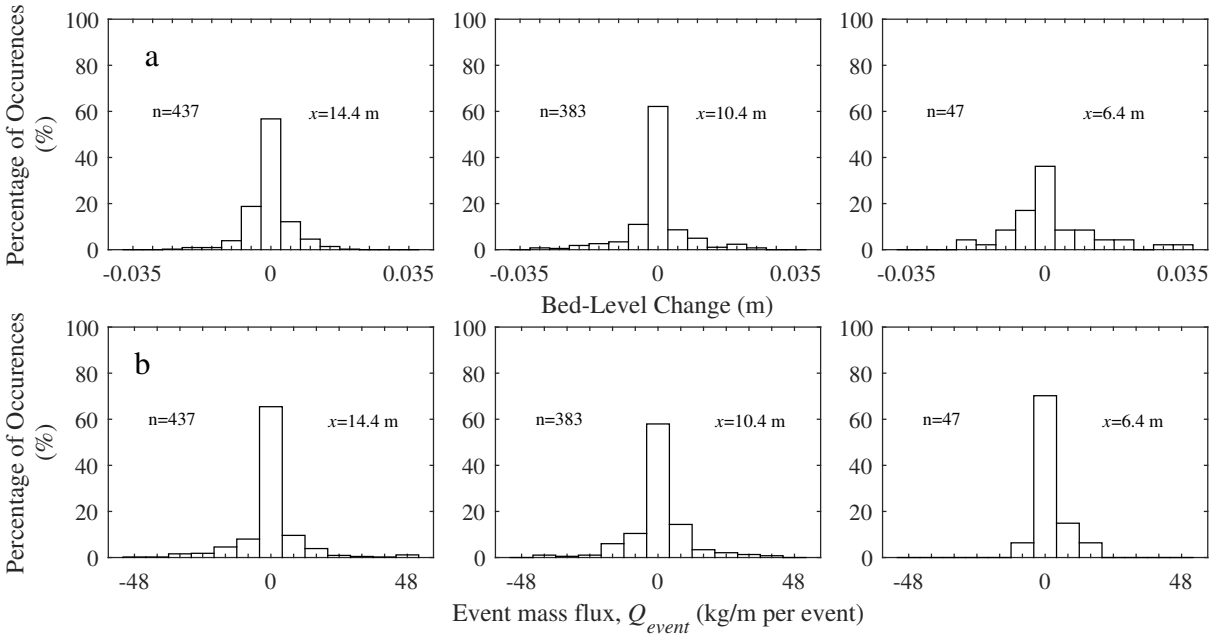

Figure 6: (a, *top row*) Percentage occurrence of bed-level changes caused by swash events at three locations on the beach face during the example tide, within ±0.035 m range. (b, *bottom row*) Percentage occurrence of event mass fluxes at three locations on the beach face during the example tide, within ±52 kg/m range. In each panel, the number of swash events n and the corresponding cross-shore position are indicated.

event-by-event bed level changes measured every 12 s (corresponding mean offshore peak period), and then averaged over ten-minute windows. The net volume change is a way to quantify the net change in revetment morphology between time t and *t+10 min* minutes. The gross volume change is used as a way to indicate the total amount of sediment transport over a ten-minute period, by summing every change occurring between all t and *t+12 s* periods contained in a ten-minute window.

Figure 7a shows the net and gross rate of bed volume change (in m^2/s) over the course of the example tide. It shows that both rates increase and decrease with the water level. This can be explained by the fact that the surf zone at North Cove is highly dissipative at all tide levels when the wave height is large. Thus, the surf zone is saturated in energy and the energy reaching the revetment depends on the water level. This is illustrated in Figure 8, which shows that the wave height at the toe of the revetment is a function of the water depth at the toe, as observed by Blenkinsopp et al. (2022b) for composite beaches and dynamic cobble berm revetments. Thus the energy available to mobilise cobbles and produce bed volume change is directly related to the water depth at the toe.

Figure 7b shows that the ratio between the gross and net rate varies between 2 and 8. Note that similar values were observed for all recorded tides, and this is close to the ratio of 10 measured in prototype scale laboratory testing by Bayle et al. (2020) on a dynamic cobble berm revetment composed of rounded and well-sorted cobbles with $D_{50} = 6.4$ cm. This ratio shows that the revetment elevation is constantly changing over ten minutes, but that the final magnitude of net change is 2 to 8 times smaller than the sum of the absolute positive and negative changes which cause it. In other words, the cobbles composing the revetment show a highly-dynamic behaviour, moving both seaward and landward throughout the tide. However, because it was shown in Figure 6 that the flux distribution at all points on the revetment was

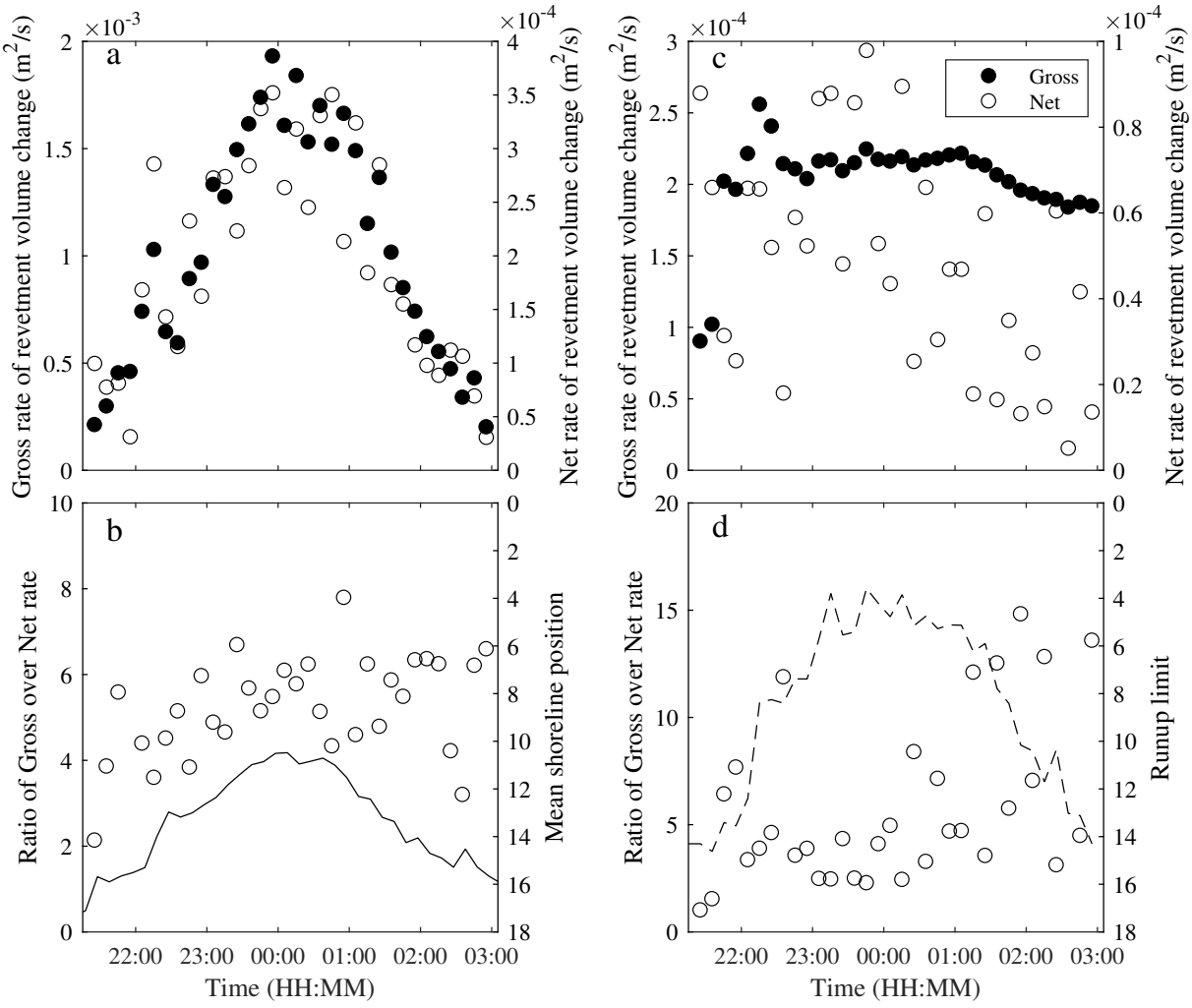

Figure 7: *Top panels*: Gross (filled circle) and net (empty circle) rate of bed volume change in m^2/s, per 10 minutes windows for the example tide, (a) calculated over the entire revetment profile length (18.7 m), and (c) calculated every ten minutes from the runup limit (dashed line in Figure 5) to a point four meters seaward, which represents the upper swash region. Note that two y-axes are used to present both datasets on the same figure. *Bottom panels*: Ratio of the gross over the net rate ($\overline{dV}/dV_{10}$) of bed volume change per 10 minute window for the example tide, (b) calculated over the entire revetment profile length (18.7 m), and (d) calculated every ten minutes from the runup limit to a point four meters seaward. The dashed and solid lines represent the runup limit and the mean shoreline position (measured every 10 minutes) respectively.

approximately symmetrical, the net change caused by this movement is much smaller, leading to overall stability of the revetment. Note that for most of the recorded tides, the ratio tends to be slightly smaller during the rising tide than during the falling tide.

Figure 7c examines the gross and net rate of volume change over a four-meter window bounded at the landward boundary by the averaged ten-minute runup limit (dashed black line). This method allows only the rates characterising the upper swash to be captured, as it moves up and down the revetment face over the tide. It is clear that the trend of both rates within the four-meter window is very different from the trend over the full revetment, and this is true for all recorded tides. The gross rate over the four-meter window is almost constant over the tide, with a slight decrease during the falling tide, while the net rate is more variable. The ratio of the gross over net rate, calculated over the same four-metre window and shown in Figure 7d, shows similar values as over the whole revetment (Figure 7b), except during the

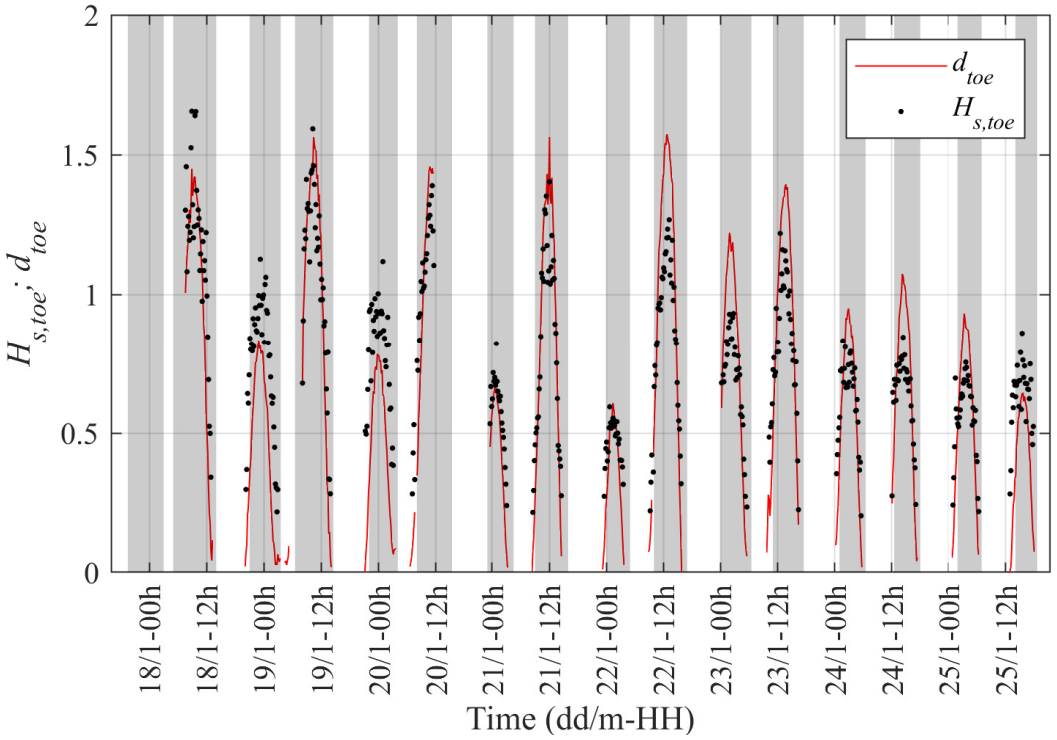

Figure 8: Time series of the significant wave height (black dots) and water depth (red line) at the toe of the revetment. These two variables were derived from the Lidar measurements when interaction between the revetment and wave/swash occurred (grey shaded areas).

falling tide when it reaches values between 15 and 20. Note that this is the case for all recorded tides. Given that over the four-metre window, the gross rate is approximately constant and always larger than the net rate, this increasing ratio can only be due to a decrease in net rate. This is further confirmed by computing the total gross rate over the whole swash zone divided by the four-meter window gross rate, and the total net rate divided by the four-meter window net rate (i.e., values in Figure 7a divided by values in Figure 7c). The gross rate ratio varies from 1 at low tide to 9 at high tide, and it is correlated with the tidal elevation hence the amount of revetment area covered by the swash. The net rate ratio also has a value of 1 at low tide, but its maximum (12) occurs during the first couple of hours of the falling tide. This confirms that the net changes caused by the upper part of the swash decrease during the falling tide, contributing less to the total net change.

This analysis shows that during the rising tide when the energy reaching the revetment increases (Figure 8), the revetment rapidly reshapes but then remains relatively stable under the action of the upper part of the swash as the tide recedes. This suggests that under increasing wave forcing, the revetment globally evolves to a different shape before reaching a relative stability, however the overall movement of cobbles (gross rate) always remains important. At the intra-tidal scale, this is consistent with the study of Bayle et al. (2020) who observed that the front slope of a dynamic cobble berm revetment at prototype scale can substantially reshape and change within 20 minutes or less under the action of waves, and then remain almost unchanged. At the inter-tidal scale, this is consistent with Bayle et al. (2021) who observed that the current revetment adjust to new wave forcing over a few tides, before being

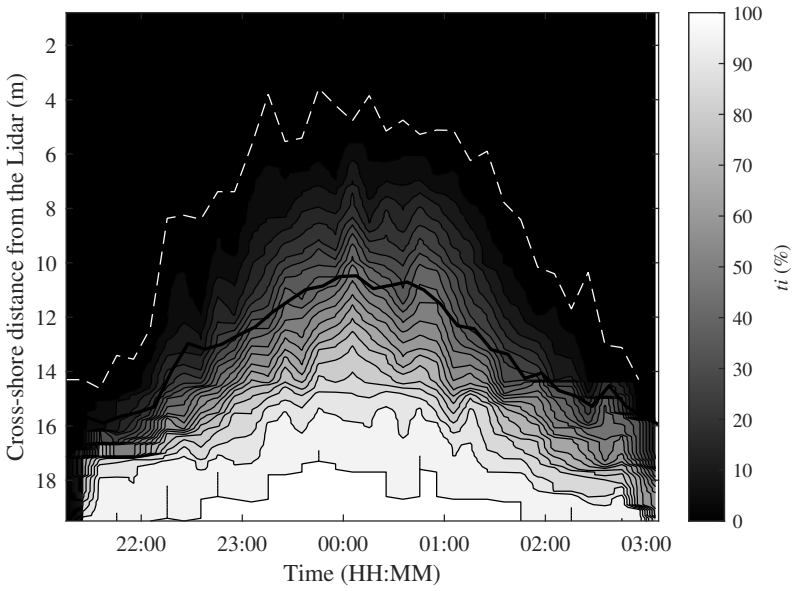

Figure 9: Contour plot showing the distribution of the percentage of time that the bed is inundated, t_i as a function of time during the example tide. Percentage of bed inundation was calculated as a ten–minute average. The dashed white and thick black lines represent the runup limit and the mean shoreline position respectively.

relatively stable under that forcing.

3.2. Bulk analysis of swash characteristics

In this section, all periods when the swash zone coincided with the dynamic revetment (mid to high tides shown using grey shaded bands in Figure 3) are used to analyse swash-induced mass fluxes and swash depth characteristics over the spring tidal cycle. The magnitude of fluxes at a specific point on the beach are dependent on the position of the swash zone, and hence vary with the water level (Figure 3c and Figure 8). To remove this spatial bias from the analysis of fluxes, the percentage of time that the bed is inundated (t_i) at each 0.1 m grid point is used to indicate relative position within the swash zone (*e.g.*, Blenkinsopp et al., 2011; Masselink et al., 2009, 2005; Aagaard & Hughes, 2006; Masselink & Russell, 2006). The percentage inundation t_i was calculated over ten-minute time windows for all tides. Figure 9 shows a contour plot illustrating the percentage of bed inundation t_i over the revetment for the example tide. Note that because the revetment surface is irregular due to the cobble surface, it is possible to have an inundated point landward of a dry point at the same time step. This is particularly the case at the bottom of the revetment, where large cobbles are common and can protrude through the water surface, but this does not affect the analysis.

3.2.1. Swash-induced event mass fluxes spatial variations

To investigate the relationship between the inundation-normalised cross-shore position and the event mass fluxes, every measured event mass flux was assigned to a percentage inundation class based on the value of t_i at the time of occurrence, with a class size of 10 % bed inundation ranging from $0-10$ % to $90-100$ %. Figure 10 shows that while the data in all classes are approximately symmetrically distributed, a distinct spatial variation in the magnitude of event mass fluxes is evident. The variation evolves from a peaked distribution in the upper swash, with more than 60 % of events within the range $\pm 4\,\mathrm{kg/m}$ per

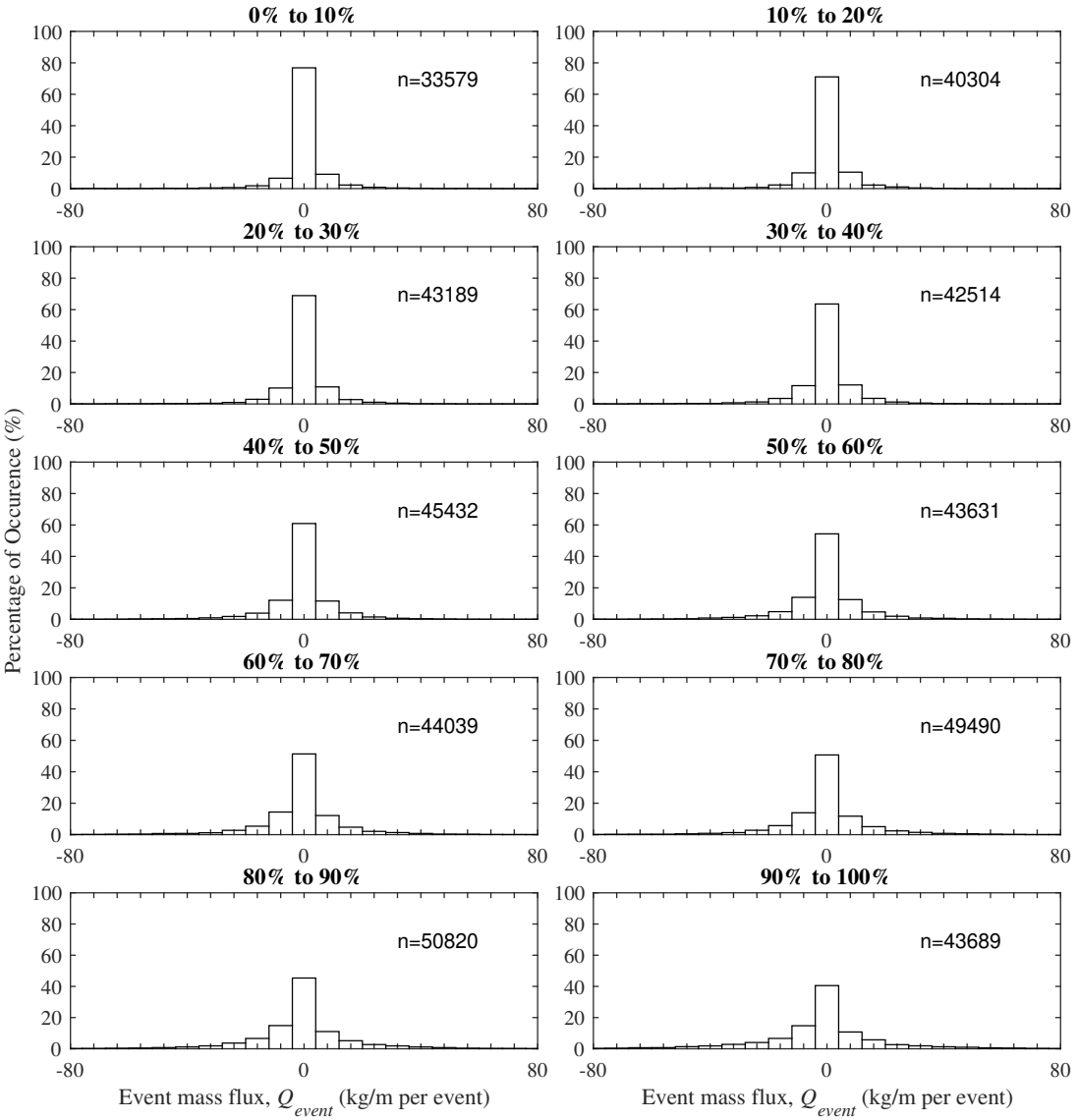

Figure 10: Percentage occurrence of event mass fluxes grouped in terms of percentage inundation, t_i for all tides recorded by the lidar. The number of swash events n used for each histogram is included on the plot, and is relatively high due to the spatial coverage of the lidar, which gives one data point every 0.1 m.

event, to a broader distribution in the lower swash zone, with $60-70$ % of fluxes of magnitude larger than 4 kg/m. This observed trend is progressive, moving seaward through the normalised swash zone, with the standard deviation increasing with the percentage of inundation window, from 10 kg/m in $0-10$ % to 25 kg/m in $90-100$ %. Again, the measurement error due to the vertical precision of the lidar yields low confidence in any quantitative interpretation of the central bar on Figure 10, although the range covered by each bar plot was increased to address this issue. The qualitative and systematic trend showing a decrease in zero-equivalent swash-induced event mass fluxes from top to bottom of the revetment remains valid and is insignificantly affected by the small measurement error.

Further investigation of the distributions of flux within each percentage inundation class for all tides is shown in Figure 11. Figure 11a presents the skewness of event mass fluxes within each class and shows that the skewness changes from high negative value to low negative value from the upper to the lower swash zone. Figure 11c presents the mean event mass flux in each percentage inundation class, while Figure 11b

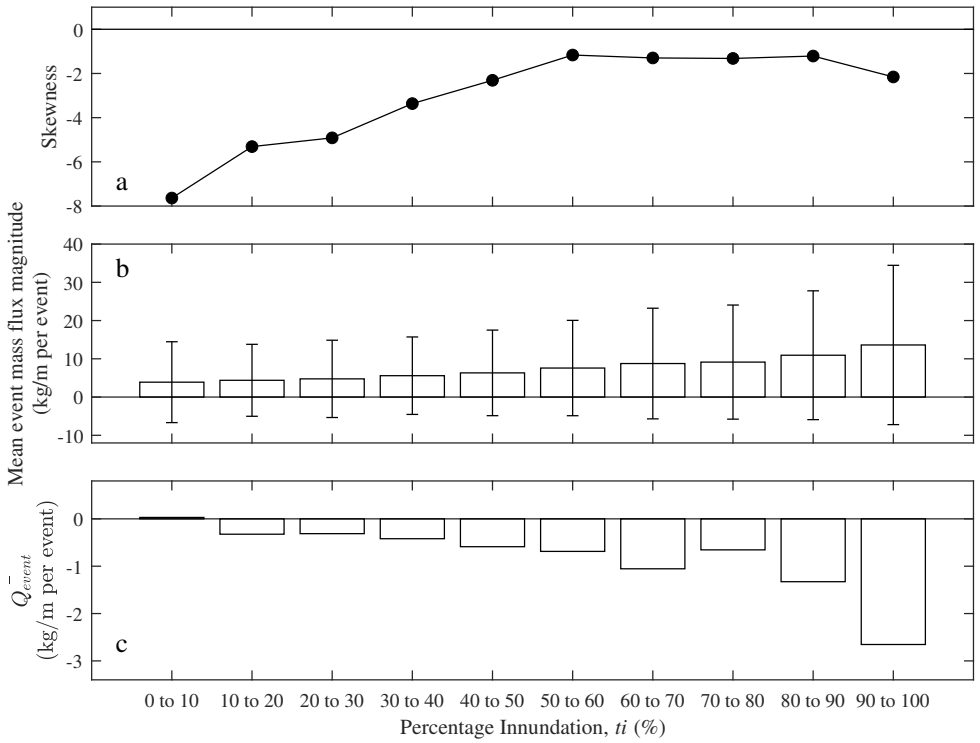

Figure 11: (a) Skewness of event mass flux distribution induced by all detected swash events; (b) mean magnitude (histogram) and standard deviation (error bar) of event mass flux; and (c) mean event mass flux, as a function of percentage inundation, t_i for all tides recorded by the lidar.

shows the mean and standard deviations of the mean event mass flux magnitude. Because the sign is removed when calculating the event mass flux magnitudes, all values are positive and approximately an order of magnitude larger than the mean values presented in Figure 11c. Figure 11b shows that both the mean and the standard deviation of the event mass flux magnitude increase with percentage inundation t_i, which is consistent with the distributions shown in Figure 10. Figure 11c shows that swash areas with $t_i > 80$ % have a high negative mean value, suggesting that material is transported seaward from these locations within the normalised swash zone. These high negative fluxes represent cobbles which are transported from the top and middle part to the lower part of the revetment, and accumulate at the revetment toe, around $x = 18 - 20$ m. They also represent erosion of the sand underneath the revetment, which was transported seaward of the revetment during the experiment as demonstrated by Bayle et al. (2021).

3.2.2. Depth of swashes

To investigate the distribution of mass fluxes further, the maximum depth of each swash event was extracted and related to the event mass flux for all cross-shore point on the revetment and all recorded events. In order to remove the effect of splashes, the depth presented is the 95^{th} percentile depth for each swash. Nonetheless, it will be referred to as the "maximum depth" for the rest of the paper. As a reminder, the calculation of the maximum depth of a swash is assessed independently from the duration of the swash – for instance, a maximum depth of 0.40 m can either represent a short swash reaching this depth once, or a longer swash attaining this depth several times. Figure 12 shows that the mean and

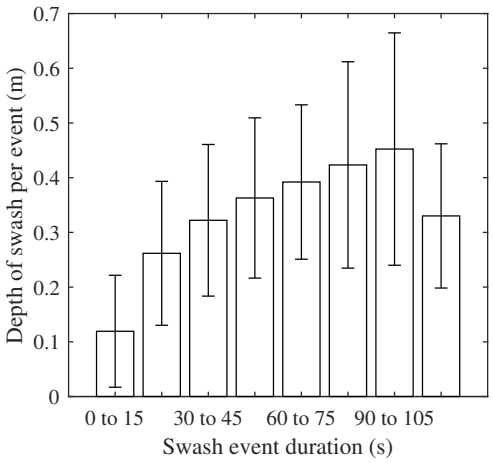

Figure 12: Mean and standard deviation (error bar) of the maximum depth of swash measured per 15 s window of swash duration.

standard deviation of the maximum depth of a swash tend to increase as the duration of a swash increases. To eliminate this temporal bias from the flux analysis, event mass flux values are presented per second in this section, and will be referred to simply as "mass flux", noted Q_s (see Section 2.4.3). The analysis of the bulk distribution of the maximum depth of individual swash events for all points on the revetment and for all tides revealed that 99 % of all swashes have a maximum depth smaller than 70 cm, with 50 % being smaller than 15 cm. Moreover, it showed that 50 % of the depth of swashes which resulted in zero net fluxes are smaller than 3 cm, and 95 % are smaller than 15 cm. For this reason, swashes smaller than 15 cm are referred to hereafter as "shallow events".

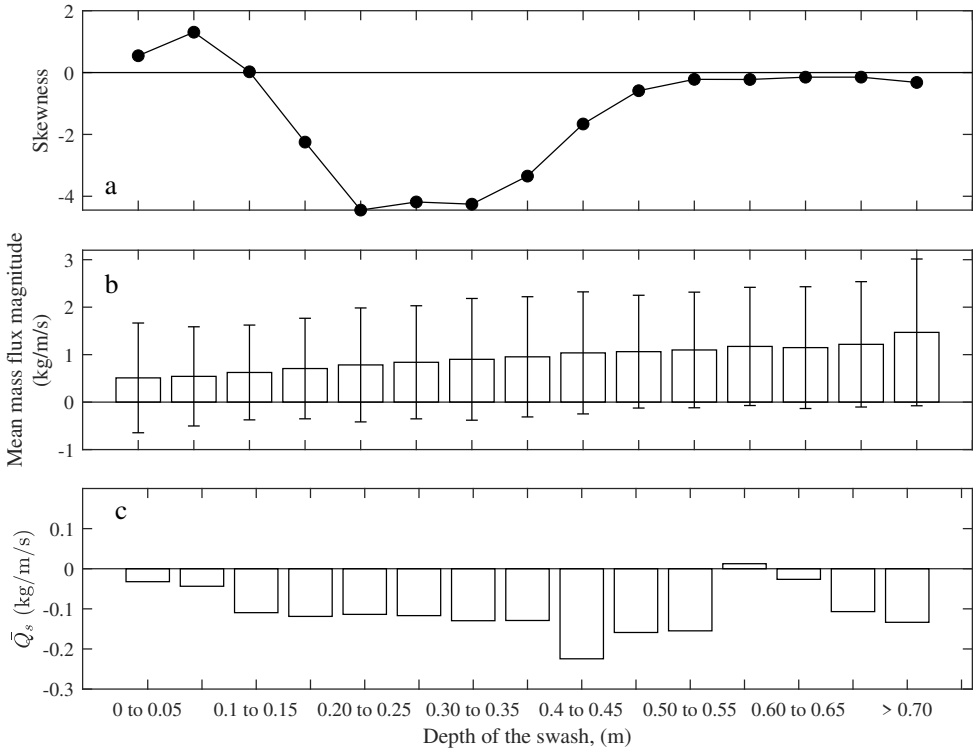

Figure 13: (a) Skewness of mass flux induced by all detected swash events; (b) mean magnitude (histogram) and standard deviation (error bar) of mass flux; and (c) Mean mass flux, as a function of the maximum depth of individual swashes. Note that the bin size increases by 0.05 m and are shown for every other tick.

Figure 13b presents the bulk mean magnitude and standard deviation of the mass fluxes (kg/m/s) as a function of the maximum depth of the associated swash event, at each point on the revetment and ranging from $0 - 0.05$ m to > 0.70 m. It shows that the mean mass flux magnitude increases with the maximum depth of swash, but the standard deviation of mass fluxes only varies from 1.2 kg/m/s in the $0 - 10$ % inundation class to 2.1 kg/m/s in the $90 - 100$ % class. This increase in mean magnitude is very similar to that shown in Figure 11b per inundation class. By contrast, the standard deviation of the magnitude is more constant with varying depth of swash than inundation class. This suggests that while event mass fluxes are of high magnitude in areas with $t_i > 80$ %, mass fluxes can be of high magnitude in areas with a maximum depth of swash of 0.20 m or larger (Figure 13b). In addition, Figure 13a shows that the mass fluxes caused by swashes with a depth between $0.15 - 0.45$ m, referred to as "mid-depth events", are negatively skewed. They also have a relatively large negative mean mass flux (Figure 13c) and generate large extreme mass fluxes with maximum magnitude of 40 kg/m/s (not shown). By contrast, events deeper than 0.45 m, referred to as "deep events", generated smaller extreme mass fluxes (maximum magnitude of 14 kg/m/s, not shown). Therefore, the part of the revetment slope inclined to undergo large extreme mass fluxes is where the mid-depth events occur, so where the swash water body has a maximum depth between $0.15 - 0.45$ m. These extreme mass fluxes likely occurred near the location of bore collapse where the energy available to initiate sediment transport is greatest. In contrast, the deep part of the swash mainly generates flows which, unlike for pure sandy beaches, do not significantly mobilise cobbles hence generate less and smaller extreme fluxes. Given this observation, plus the fact that deep events are generally long in duration (Figure 12) and that large extreme mass fluxes already occur in the mid-depth part of the swash, it is normal to measure smaller extreme mass fluxes in the deep part of the swash even though high magnitude event mass fluxes are present in areas with $t_i > 80$ %.

3.3. Cross-shore bed change oscillations

To further analyse the inundated sections of the revetment, an analysis of spatial and temporal variation of event mass fluxes over the example tide is shown in Figure 14. Figure 14a presents a timeseries of net cross-shore mass fluxes measured at a single point on the revetment ($x = 12.5$ m) determined every two–minute and ten–minute intervals. It shows that while the majority of single event fluxes at a point on the revetment cause little or no revetment mass change (Figure 6a), large onshore and offshore mass fluxes occur throughout the tide. The two lower panels in Figure 14 present contour plots of the net cross-shore mass fluxes within two–minute (Figure 14b) and ten–minute (Figure 14c) intervals. Figure 14b shows that at the two minutes sampling interval, there is evidence of oscillating periods of onshore and zero/offshore mass fluxes particularly in the lower parts of the swash zone throughout the entire duration of the tide, although periods of offshore transport are more common. This is confirmed by Figure 14c which clearly shows a tendency toward erosive periods when the fluxes are summed over ten minutes. Similar oscillations were observed on a sandy beach by Blenkinsopp et al. (2011) who suggested that they indicate the presence of a form of dynamic equilibrium caused by combination of negative feedback and short-term process dampening to limit the overall rate of morphological change. However, the relationship between these oscillations and external forcing is yet to be analysed.

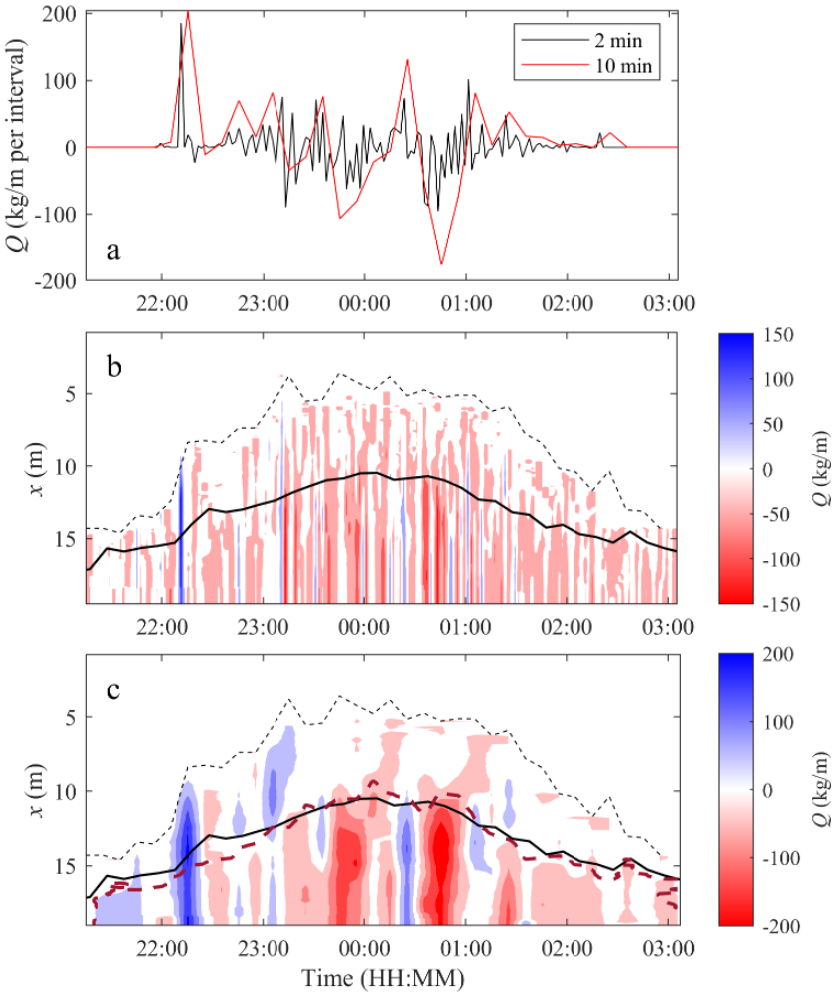

Figure 14: (a) Timeseries of net cross-shore mass flux for the example tide at two and ten–minute intervals, at $x = 12.5$ m. Contour plots of net cross-shore mass flux during the example tide summed over (b) two–minute and (c) ten–minute time windows. Note that 2 minutes was chosen as it represents the longest swash event recorded. The dashed thick line (violet) marks the cross-shore percentage of inundation limit of the flux oscillations (*e.g.*, manually estimated cross-shore limit landward of which bed oscillations are minimal in (c)), at $t_i = 40$ % for the example tide. The dashed and solid lines represent the runup limit and the mean shoreline position respectively. Note that the colour bar scale ranges between ± 150 kg/m in (b) and ± 200 kg/m in (c).

A feature of Figure 14c is that these flux oscillations tend to be weaker in the upper swash zone except during the first $1-2$ hours of the rising tide. This supports the observation made in Section 3.1.2 that the upper part of the swash is more inclined to generate net bed changes during the rising tide, suggesting profile stability in the upper part of the swash is reached relatively quickly and subsequent variability is small. The limit of these oscillations was extracted from the ten–minute period with a semi-automatised method using the net cross-shore mass flux summed over each 10 % inundation line. From the 100 % to the 0 % inundation line, the first line characterised by a rate of change negatively larger than 80 kg/m per t_i is taken as the flux oscillation limit, thus associated to an inundation percentage t_i.

For each recorded tide, the value of percentage inundation at which the oscillation limit occurred is presented as a function of the mean wave period (T_{m02}) recorded at the toe of the revetment (Figure 15). The plot shows a correlation between the relative position of this limit in the swash and the mean wave period, with a coefficient of correlation ($r^2 = 0.78$). It indicates that as the period increases (decreases),

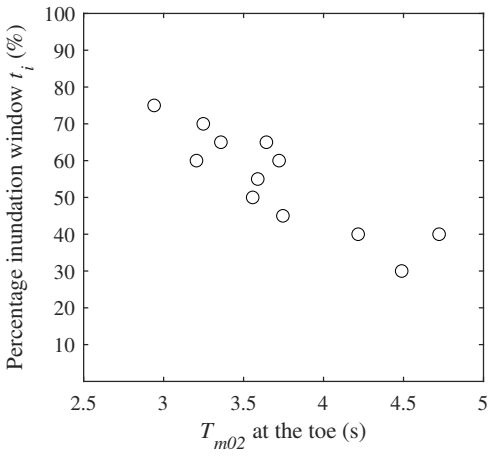

Figure 15: Plot of the flux oscillation limit (% of inundation) against the mean wave period (T_{m02}) at the toe of the revetment. Values of the Pearson r^2 correlation coefficient is 0.78.

the line of delimitation moves landward (seaward) within the normalised swash. This suggests that the longer the wave period, the greater chance of larger fluxes occurring closer to the runup limit. Locations landward of this limit are only composed of short swashes with a duration of less than 15 seconds (similar range for each recorded tide). Referring to Figure 12 shows that swashes shorter than 15 seconds are also relatively shallow. These shallow events have a small mean mass flux magnitude, with a negative mean mass flux (Figure 13b,c). For this reason, most of the mass fluxes measured above this limit are negative (Figure 14b,c), and typically lead to minimal net change over two and ten minutes time periods because the revetment is in a relatively stable state after the initial cobble rearrangements which occurred during the rising tide. Accurate data on local water level elevation during energetic events are important to set the revetment at the right elevation (more specifically, the revetment toe), and this is translated in the recently developed empirical runup equation for composite beaches by Blenkinsopp et al. (2022b).

4. Discussion

The discussion is divided into two subsections: the first discusses the results in term of sediment transport and the implication of this work in terms of dynamics revetment; the second compares the current results with those obtained for sandy beaches, focusing on a comparison with (Blenkinsopp et al., 2011) who performed very similar analysis.

4.1. Sediment transport

The swash analysis of all tides recorded during the spring tidal cycle showed that onshore and offshore fluxes almost balance over the tide and over the entire swash area. Net changes are the consequence of either the accumulation of a slight imbalance between positive and negative swashes or a few extremes events. In other words, except when a large cobble or group of cobbles is mobilised to cause a large net change, it is likely that most of the time mobilised cobbles simply readjust their position relative to each other, potentially achieving better interlocking. It is further noted that due to the large size of the sediment composing the revetment, the movement of a single stone can lead to substantial bed elevation change at a single point and it may be that a depression is left on the revetment surface which becomes

a natural location for future deposition. This helps to explain why the revetment remains a coherent structure over time and does not undergo major changes at either the intra- and inter-tidal timescale.

The majority of net morphology change at a location occurs during the rising tide as swash first reaches it. The majority of net change happens over timescales of tens of minutes with the cobble slope rapidly reaching a quasi-stable state as shown in Bayle et al. (2020). This has implications for the design of dynamic cobble berm revetments since the shape and slope will rapidly change to a quasi-equilibrium shape driven by the forcing conditions. Therefore, it is likely to be unnecessary to over-design the revetment geometry, since a relatively rough placement is expected to rapidly reshape to an "deterministic" quasi–equilibrium shape and slope under swash action. However, it will be necessary to ensure that sufficient cobble volume is available for this shape to be formed. To aid the specification of cobble volume, Blenkinsopp et al. (2022b) presents measurements of quasi-stable revetment slopes in the range 1:3 to 1:8 and provide a method to estimate wave runup on dynamic revetments which can be used to determine the expected crest elevation.

Small bed changes also possibly represent changes in the sand within or underlying the revetment, as observed in Bayle et al. (2021), through sand erosion (*i.e.*, winnowing caused by the backwash water) and sand compaction (kinetic sieving), although the latter is generally a slower process. The water table is thought to be of importance in the underlying sand dynamics, as presented by Kulkarni et al. (2004) for a mixed beach. However, unlike mixed beaches, composite beaches and dynamic cobble berm revetments have a natural underlying filter layer of mixed sand and gravel (Figure 4) at the "runoff interface" defined in the conceptual model of Bayle et al. (2021), which limits the underlying sand erosion. Nonetheless, during the rising tide, the water table rises but remains at the sand-cobble interface or below, and remains below the area affected directly by the upper swash. Therefore, the upper swash percolating through the cobbles reaches unsaturated sand, with empty void spaces into which water can infiltrate, promoting erosion of the underlying sand as water drains back out through the revetment. The water table reaches its maximum at high tide, and remains relatively higher during the falling tide than the rising tide due to capillarity. As a consequence, during the falling tide, the upper swash percolating through cobbles reaches a saturated sand/filter layer with less free void space, resulting in less infiltration and hence reduced sand mobilisation as the water flows seaward at the runoff interface. The dynamics of both sediment types (sand and gravel) detailed above explains why the rising tide generates globally more net change in the upper part of the swash than the falling tide. This highlights at the swash scale the importance of the naturally formed mixed sand and cobble filter layer where the "runoff interface" develops. For the poorly-sorted and angular material used for the structure reported on here, this filter layer built up naturally at the study site. It is not clear whether this filter layer should be a design feature so that it is present immediately after construction, or whether to simply allow natural sorting over time. To gain clarity, the time taken for this natural sorting requires further investigation now that the process has been identified. This sorting is also very likely related to the thickness of the cobble layer mobilised by the swash, and this also needs to be investigated.

This study also showed that while mean event mass fluxes are high in the inundation zone $t_i > 80$ %, the analysis of the maximum depth of swash recorded per inundation class (not shown) revealed that

overall, deep events ($> 0.45\,\mathrm{m}$) only occurred in areas inundated more than 50 % of the time. By contrast, it was identified that the largest extreme mass fluxes occurred where the swash reaches a maximum depth between $0.15 - 0.45\,\mathrm{m}$. As a consequence, extreme net changes occurring in the upper swash during the rising tide (Section 3.1.2) are likely located where the swash reaches depths between $0.15 - 0.45\,\mathrm{m}$.

4.2. Comparison with sandy beaches

The present results suggest strong similarities with sandy beaches in terms of sediment transport in the swash zone. It was showed that a single swash event can produce large changes of the order of magnitude of the cobble diameter $D_{50} = 15\,\mathrm{cm}$, but that in general, these events are rare. These large events are also three to six times larger than those observed on sandy beaches (Blenkinsopp et al., 2011; Baldock et al., 2006; Turner et al., 2008), which may be expected on a dynamic cobble berm revetment as the movement of a single cobble can significantly change the bed elevation at a point on the surface. The percentage of inundation distribution of swash-induced fluxes (Figure 10) was very similar to that measured on sandy beaches by Blenkinsopp et al. (2011) and suggests that the inundation variability of swash-induced fluxes are independent of the bed-type. Furthermore, the bed change oscillation pattern presented in Section 4.1 was also observed on a sandy beach by Blenkinsopp et al. (2011), which confirms a degree of independence from the bed-type. In addition, the enhanced net bed level changes in the upper part of the swash during the rising tide is also observed on a sandy beach, but to a lower degree.

Event mass fluxes, both for the mean and extreme events, are around 20 % smaller than those observed on sandy beaches (Puleo, 2009; Masselink et al., 2009; Blenkinsopp et al., 2011). The majority of event mass fluxes measured on the dynamic revetment and previously observed on sandy beaches are in the $\pm 10\,\mathrm{kg/m}$ range. However, overall, cobbles are less mobile but a small movement can cause a much larger change due to the size of particles. Generally, the smaller fluxes per event measured on the revetment compared to sandy beaches supports the idea that the revetment is more stable and resistant to wave attack than a sandy beach.

Figure 7 also showed that the revetment is able to rapidly reshape and reach a relatively stable shape during the rising tide, resulting in a decrease in net change after the first interactions with the upper swash. To extend this, the ratio of the net flux (Q_{net}) to the sum of absolute fluxes (Q_{abs}) from all individual swashes at the maximum mean shoreline position over the course of each tide was calculated (not shown). It is observed that the net cross-shore mass flux is on average 18 times smaller than the absolute cross-shore mass flux. Using the same method, Blenkinsopp et al. (2011) measured net mass fluxes that were on average 63 times smaller than the absolute fluxes for sandy beaches. The smaller values of this ratio measured on the dynamic revetment suggest that there is relatively less sediment movement on a wave-by-wave timescale than on a sandy beach. Cobbles composing the revetment are hard to bring in motion but have the potential to cause lots of change if they are moved, while with sand initiation of motion is easier but a lot of particles have to be moved to cause significant changes.

The relatively small variability in the revetment geometry even when subjected to large waves, high water levels and powerful swash events is useful information for coastal engineers. By giving information on how much the revetment volume and shape changes over the course of a high tide (typically by no

more than ± 0.2 m, Figure 5, so about one or two layer of pure cobble), the measurements presented here suggest that it is not necessary to add a very large volume of cobbles to the revetment face to cope with this variability and prevent exposure of the underlying sand surface. While the revetment in its current state provides efficient protection of the sand scarp during energetic events (Bayle et al., 2021), long-term analysis of its behaviour under extreme conditions and longshore sediment transport is required to fully assess its performance and resilience.

5. Conclusion

The dynamic revetment at North Cove (WA, USA) was monitored over nine days in January 2019, corresponding to almost a spring tidal cycle. The swash zone was continuously monitored using a 2-D lidar, and these high-resolution measurements were for the first time used on dynamic revetment (and composite beach) to assess the cross-shore mass fluxes of material moved by individual swash events.

The analysis of bed-level changes and net cross-shore mass fluxes over the revetment demonstrated that revetment changes were mainly driven by very small events (± 3 cm and ± 50 kg/m), with some rare large bed-level changes of a magnitude similar to the median cobble diameter ($D_{50} = 0.15$ m).

For every tide, the distribution of event mass fluxes was nearly symmetrical, with positive and negative fluxes tended to balance out over a tide, meaning that the revetment was constantly changing but stable. The revetment underwent relatively more net change during the rising than the falling tide, with the upper part of the swash causing the main net changes toward a relatively stable state. This was hypothesised to be due to the combination of groundwater infiltration and water table elevation, as well as the presence of a runoff interface, a feature for composite beaches and dynamic revetments. Furthermore, it was also shown that over a tide, the absolute sum of all fluxes at the maximum mean water was on average 18 times larger than the magnitude of the net flux at the same point. Some very generic design guidelines are suggested for the design and instalment of dynamic cobble berm revetment.

The analysis of event mass fluxes as a function of percentage inundation showed that areas with $t_i > 80$ % are subject to large mean event mass flux. In parallel, the analysis of net cross-shore mass flux per second revealed that the revetment section where the swash reached a maximum depth between $0.15 - 0.45$ m undergoes the more extreme fluxes. Swashes deeper than 0.45 m only occurred in zones inundated more than 50 % of the time, and smaller extreme fluxes were measured over the corresponding section of the revetment.

Flux oscillations were observed as for sandy beaches, and the cross shore limit of these, detected over the ten–minute windows, was correlated with the mean wave period at the toe of the revetment. Overall, the water depth at the toe of the revetment played an important role in the amount of energy that reaches the revetment, as the surf zone is often saturated during energetic events.

Future work should focus on a way to monitor the vertical interface between sand and cobbles at a high spatial and temporal resolution. Although it was identified that both materials were mobilised by swashes, the event-by-event dynamics of this interface remains unclear, and the separation of both components remains a challenge.

Acknowledgements

Funding: Paul Bayle is supported by a PhD scholarship through the EPSRC CDT in Water Informatics: Science & Engineering (WISE). Travelling and living fees associated with this experiment were partially covered by a Santander Mobility Grant, obtained via the University of Bath.

The authors want to thank the entire Washington Department of Ecology CMAP team, for their logistical support in the field. The authors would also like to thank the community of North Cove for their warm welcome and support throughout the experiment. Special thanks to Richard and Dianne Harris for providing a warm and dry place during the experiment, and to Connie Allen for organising the communication and public relations around the experiment. Finally, we thank William Bazeley, Neil Price, Robert Dyer and David Surgenor from the University of Bath for their technical support during the experiment preparation.

References

Aagaard, T., & Hughes, M. G. (2006). Sediment suspension and turbulence in the swash zone of dissipative beaches. *Marine Geology*, *228*, 117 – 135.

Ahrens, J. P. (1990). Dynamic revetment. *Coastal Engineering*, *138*, 1837 – 1850.

Allan, J. C., & Gabel, L. L. (2016). *Monitoring the response and efficacy of a dynamic revetment constructed adjacent to the columbia river south jetty, Clatsop county, Oregon.*. Technical Report O-16-07 Oregon Department of Geology and Mineral Industries.

Allan, J. C., Geitgey, R., & Hart, R. (2005). Dynamic revetments for coastal erosion stabilization: a feasible analysis for application on the oregon coast. *Oregon Department of Geology and Mineral Industries*, *Special issue, 37*.

Allan, J. C., Harris, E., Stephensen, S., Politano, V., Laboratory, H., Folger, C., & Nelson, W. (2012). *Hatfield Marine Science Center Dynamic Revetment Project*. Technical Report Hatfield Marine Science Center, Oregon State University.

Allan, J. C., Hart, R., & Tranquili, J. V. (2006). The use of passive integrated transponder (pit) tags to trace cobble transport in a mixed sand-and-gravel beach on the high-energy oregon coast, usa. *Marine Geology*, *232*.

Allan, J. C., & Komar, P. D. (2002). Extreme storms in the pacific northwest coast during the 1997–98 el niño and 1998–99 la niña. *Journal of Coastal Research*, *18*, 175 – 193.

Almeida, L. P., Masselink, G., Russel, P. E., & Davidson, M. A. (2015). Observations of gravel beach dynamics during high energy wave conditions using a laser scanner. *Geomorphology*, *228*, 15 – 27.

Baldock, T. E., Barnes, M. P., & Hughes, M. G. (2006). Field observations of instantaneous cross-shore free surface profiles and flow depths in the swash zone. In *Coastal Dynamics 2005 : State of the Practice*.

Bayle, P. M., Blenkinsopp, C. E., Conley, D., Masselink, G., Beuzen, T., & Almar, R. (2020). Performance of a dynamic cobble berm revetment for coastal protection, under increasing water level. *Coastal Engineering*, *159*.

Bayle, P. M., Kaminsky, G., Blenkinsopp, C. E., Weiner, H., & Cottrell, D. (2021). Behaviour and performance of a dynamic cobble berm revetment during a spring tidal cycle in north cove, washington, usa. *Coastal Engineering*, *167*.

Blenkinsopp, C. E., Baldock, T. E., Bayle, P. M., Foss, O., Almeida, L. P., & Schimmels, S. (2022a). Remote sensing of wave overtopping on dynamic coastal structures. *Remote Sensing*, *14*, 513.

Blenkinsopp, C. E., Bayle, P. M., Martins, K., Foss, O. W., Almeida, L. P., Kaminsky, G. M., Schimmels, S., & Matsumoto, H. (2022b). Wave runup on composite beaches and dynamic cobble berm revetments. *Coastal Engineering*, *176*.

Blenkinsopp, C. E., Mole, M. A., Turner, I. L., & Peirson, W. L. (2010). Measurements of the time-varying free-surface profile across the swash zone obtained using an industrial lidar. *Coastal Engineering*, *57*, 1059 – 1065.

Blenkinsopp, C. E., Turner, I. L., Masselink, G., & Russell, P. E. (2011). Swash zone sediment fluxes: Field observations. *Coastal Engineering*, *58*, 28 – 44.

Bluck, B. J. (1967). Sedimentation of beach gravels: Examples from south wales. *Journal of Sedimentary Petrology*, *37*, 128 – 156.

Carter, R. W. G., & Orford, J. D. (1984). Coarse clastic barrier beaches: a discussion of the distinctive dynamic and morphosedimentary characteristics. *Marine Geology*, *60*, 377 – 389.

Holland, A. (2019). *Mixed sand and gravel beaches: accurate measurement of active layer depth to develop predictive models of sediment transport*. Ph.D. thesis University of Sussex.

Hughes, M. G., & Moseley, A. S. (2007). Hydrokinematic regions within the swash zone. *Continental Shelf Research*, *27*, 2000 – 2013. doi:10.1016/j.csr.2007.04.005.

Jennings, R., & Schulmeister, J. (2002). A field based classification scheme for gravel beaches. *Marine Geology*, *186*, 611 – 228.

Jennings, R., & Shulmeister, J. (2002). A field based classification scheme for gravel beaches. *Marine Geology*, *186*, 211 – 228.

Kaminsky, G., Cottrell, D., & Glore, G. (2020). Nature-based dynamic revetment construction at north cove, washington, usa. In *Coastal Engineering Proceedings, 36v*.

Kaminsky, G. M., Ruggiero, P., Buijsman, M. C., McCandless, D., & Gelfenbaum, G. (2010). Historical evolution of the columbia river littoral cell. *Marine Geology*, *273*, 96 – 126.

Kirk, R. M. (1980). Mixed sand and gravel beaches: morphology, processes and sediments. *Progress in Physical Geography: Earth and Environment*, *4*, 189 – 210. doi:10.1177/030913338000400203.

Komar, P., & Allan, J. C. (2010). Design with nature strategies for shore protection - the construction of a cobble berm and artificial dune in an oregon state park. In *Puget Sound Shorelines and the Impacts of Armoring—Proceedings of a State of the Science Workshop* (pp. 117 – 126). U.S. Geological Survey Scientific Investigations Report 2010-5254.

Kulkarni, C. D., Levoy, F., Monfort, O., & Miles, J. (2004). Morphological variations of a mixed sediment beachface (teignmouth, uk). *Continental Shelf Research*, *24*, 1203 – 1218.

Lesser, G. R. (2009). *An Approach to Medium-term Coastal Morphological Modelling*. Ph.D. thesis University of Canterbury, New Zealand.

Loman, G. J. A., van Gent, M. R. A., & Markvoort, J. W. (2010). Physical model testing of an innovative cobble shore, part i: Verification of cross-shore profile deformation. In *Third International Conference on the Application of Physical Modelling to Port and Coastal Protection*.

Lorang, M. S. (1991). An artificial perch-gravel beach as a shore protection structure. In *Coastal Sediments '91* (pp. 1916 – 1925). Reston, Va., American Society of Civil Engineers volume 2.

Martins, K., Blenkinsopp, C. E., Power, H. E., Bruder, B., Puleo, J. A., & Bergsma, E. W. J. (2017). High-resolution monitoring of wave transformation in the surf zone using a LiDAR scanner array. *Coastal Engineering*, *128*, 37 – 43. doi:10.1016/j.coastaleng.2017.07.007.

Martins, K., Blenkinsopp, C. E., & Zang, J. (2016). Monitoring individual wave characteristics in the inner surf with a 2-dimensional laser scanner (LiDAR). *Journal of Sensors*, (pp. 1 – 11). doi:10.1155/2016/7965431.

Masselink, G., Evans, D., Hughes, M. G., & Russell, P. E. (2005). Suspended sediment transport in the swash zone of a dissipative beach. *Marine Geology*, *216*, 169 – 189.

Masselink, G., & Russell, P. E. (2006). Flow velocities, sediment transport and morphological change in the swash zone of two contrasting beaches. *Marine Geology*, *227*, 227 – 240.

Masselink, G., Russell, P. E., Turner, I. L., & Blenkinsopp, C. E. (2009). Net sediment transport and morphological change in the swash zone of a high-energy sandy beach from swash event to tidal cycle time-scales. *Marine Geology*, *267*, 18 – 35.

van der Meer, J. W., & Pilarczyk, K. W. (1986). Dynamic stability of rock slopes and gravel beaches. *Coastal Engineering*, *125*, 1713 – 1726.

Michalsen, D. R. (2018). *Feasibility of long-term shoreline stabilisation alternatives between North Cove and Tokeland, WA*. Technical Report U.S. Army Corps of Engineers, Seattle District.

Orford, J. D. (1975). Discrimination of particle zonation on a pebble beach. *Sedimentology*, *22*, 441 – 463.

Poate, T., Masselink, G., McCall, R., & Russell, P. E. (2015). Uk storms 2014: Gravel beach response. In *Coastal Sediments 2015*.

Powell, K. A. (1988). The dynamic response of shingle beaches to random waves. *Coastal Engineering*, *130*, 1763 – 1773.

Puleo, J. A. (2009). Tidal variability of swash zone sediment suspension and transport. *Journal of Coastal Research*, *25*, 937 – 948.

Pye, K., & Blott, S. J. (2018). *Advice on Sustainable Management of Coastal Shingle Resources*. Technical Report 273 Natural Resources Wales.

Ruggiero, P., Kaminsky, G. M., Gelfenbaum, G., & Voigt, B. (2005). Seasonal to interannual morphodynamics along a high-energy dissipative littoral cell. *Journal of Coastal Research*, *21*, 553 – 578.

Sallenger, A. H. (2000). Storm impact scale for barrier islands. *Journal of Coastal Research*, *16*, 890 – 895.

Turner, I. L., Russel, P. E., & Butt, T. (2008). Measurement of wave-by-wave bed-levels in the swash zone. *Coastal Engineering*, *55*, 1237 – 1242.

Turner, I. L., Russell, P. E., Butt, T., Blenkinsopp, C. E., & Masselink, G. (2009). In-situ estimates of net sediment flux per swash: Reply to discussion by t.e. baldock 'measurement of wave-by-wave bed-levels in the swash zone'. *Coastal Engineering*, *56*, 1009 – 1012.

Van Rijn, L. C. (2010). *Modelling erosion of gravel/shingle beaches and barriers*. Technical Report D13b European Commission, Conscience.

Ward, D. L., & Ahrens, J. P. (1992). *Laboratory study of a dynamic berm revetment*. Technical Report US Army Corps of Engineers.

Weiner, H. M., Kaminsky, G. M., Hacking, A., & McCandless, D. (2019). *North Cove Dynamic Revetment Monitoring: Winter 2018-2019*. Technical Report 19-06-008 Shorelands and Environmental Assistance Program, Washington State Department of Ecology, Olympia, WA.

Williams, A. T., & Caldwell, N. E. (1988). Particle size and shape in pebble-beach sedimentation. *Marine Geology*, *82*, 199 – 215.

Williams, J., Masseling, G., Buscombe, D., Turner, I., Matias, A., Ferreira, O., Bradbury, A., Metje, N., Coates, L., Chapman, D., Thompson, C., Albers, T., & Pan, S. (2009). Bardex (barrier dynamics experiment): Taking the beach into the laboratory. *Journal of Coastal Research*, *56*, 156 – 162.

Wright, L. D., Short, A. D., & Nielsen, P. (1982). *Morphodynamics of high energy beaches and surf zones: A brief synthesis.*. Technical Report 82/5 Coastal Study Unit, University of Sydney.